JOURNAL OF GEOPHYSICAL RESEARCH, VOL. 106, NO. C6, PAGES 11,659–11,676, JUNE 15, 2001

Breaking probabilities for dominant surface waves on water of finite constant depth

Alexander V. Babanin[1]
School of Civil Engineering, University College, The University of New South Wales, Canberra, A.C.T., Australia

Ian R. Young
Faculty of Engineering, Computer and Mathematical Sciences, Adelaide University, Adelaide, South Australia, Australia

Michael L. Banner
School of Mathematics, The University of New South Wales, Sydney, New South Wales, Australia

Abstract. This paper extends our previous study of the breaking probability of dominant deep water gravity surface waves into the finite water depth environment. It reports a unified behavior of the mean breaking statistics once the effects of finite water depth are taken into account. The shallow water wave data that form the basis of this study were acquired at a field experiment site at Lake George, New South Wales, Australia. The breaking events were detected through visual observation of videotaped records of the wave field in combination with acoustic signatures of the breaking waves from a collocated hydrophone. Following *Banner et al.* [2000], we argue that when constant finite depth bottom influence is operative, nonlinear hydrodynamical effects associated with energy and momentum fluxes within deforming wave groups remain the primary determinant of breaking onset. This underpins our proposed finite depth water parameterization for the environmental dependence of dominant wave breaking probability, given by the average number of breakers passing a fixed point per dominant wave period. The additional influence of bottom interaction with the wind drift current shear and wind forcing are also included in our finite constant depth formulation. This is a natural extension of our recently proposed deep water dependence and reduces to it as the significant wave height becomes much smaller than the water depth. In common with the deep water case we propose that there exists a threshold of the significant peak steepness below which negligible dominant wave breaking occurs. The available data show encouraging agreement with our proposed dependence, with a correlation coefficient approaching 0.9

1. Introduction

[*Banner et al.*, 2000] (hereinafter referred to as *BBY*) used the results of numerical simulations of wave- breaking onset by *Dold and Peregrine* [1986] and *Banner and Tian* [1998] as the basis of our proposed functional dependence of the breaking probability of dominant deep water waves on environmental conditions. The key elements were (1) the existence of a threshold of a predominantly hydrodynamic parameter, the significant wave steepness, below which breaking does not occur and (2) a rapid increase of breaking probability above this threshold. Model calculations of nonlinear wave train behavior provided us with insight into other possible mechanisms that influence breaking onset and their relative strengths. These mechanisms were parameterized and included in our functional form.

The physical basis of our formulation arose from studies of the evolution of deep water wave groups comprised of a fundamental carrier wave with small upper and lower sideband components, using as parameters the initial carrier wave slope $(ak)_0$ and the number of waves in one modulation length, N. *Dold and Peregrine* [1986] showed that for a given N, breaking al-

[1]Current affiliation: Department of Civil and Environmental Engineering, Adelaide University, Adelaide, Australia

Paper number 2000JC000215.
0148-0227/01/2000JC000215$09.00

ways occurs above an initial slope $(ak)_0$ threshold, and below it a recurrence occurs toward the original wave group. The initial carrier threshold wave slope $(ak)_0$ depends only weakly on the number of waves in the group N and is almost constant for $N > 4$. *Banner and Tian* [1998] also found that the presence of a superposed linear background shear current, typical of the ocean surface layer, marginally reduced the local wave slope at breaking. Our subsequent unpublished calculations have shown that wind forcing imposed over deep water wave trains marginally increases the steepness at breaking, while the combined influence of wind forcing and shear tends to cancel each other, leaving the mean dominant wave steepness, reflecting the nonlinearity of the group structure of the wave field, as the primary hydrodynamic property controlling the onset of breaking of the dominant sea waves.

The experimental data that were used to validate our proposed deep water statistical breaking dependence encompassed a particularly wide range of deep water wave conditions. These data included Lake Washington waves forced by light winds (peak frequency $f_p > 0.5$ Hz, wavelengths < 6 m), Black Sea waves typical of open seas ($f_p = 0.2 \sim 0.4$ Hz and wave lengths around $30 \sim 40$ m), and Southern Ocean storm waves with up to nearly 300 m wavelength ($f_p < 0.1$ Hz) with mean U_{10} wind speeds ranging up to 20 m s^{-1}.

Both *Gemmrich and Farmer* [1999] and BBY reported that the traditionally adopted dependence in terms of a wind forcing parameter, such as the wind speed [e.g., *Wu*, 1979; *Thorpe and Humphries*; 1980, *Xu et al.*; 1986, *Katsaros and Atakturk*, 1992], shows serious inconsistencies when examined over a broad range of wind-wave conditions. In strong contrast, BBY showed that breaking probabilities from the three very disparate sites demonstrated similar behavior when parameterized on the basis of our hypothesis that nonlinear hydrodynamic processes associated with wave groups underlie the onset of breaking. Including the effects of the surface layer wind drift current and the wind forcing was found to improve the correlation only marginally. The observed mean dominant wave breaking probability was analyzed in terms of a composite parameter based on the significant dominant wave steepness and the strengths of the surface layer shear current and wind forcing. Our proposed dependence provides quantitative prediction of the expected mean number of breakers at the spectral peak per dominant wave period. The dependence features a common threshold of the steepness parameter below which negligible dominant wave breaking occurs, with a near-quadratic dependence of the breaking probability once this threshold is exceeded.

For the present case of waves in finite constant water depth an additional bottom interaction is imposed on the orbital velocities of steep waves due to close proximity of the bottom. To our knowledge, no detailed modeling of bottom influence on wave train evolution to breaking has yet been reported. As a first step, we propose a parameterization of the bottom influence on the composite parameter through a term that quantifies the significant wave height relative to the mean water depth. In the deep water limit this relative depth parameter approaches unity, and our proposed finite depth breaking probability dependence reduces to the deep water dependence proposed by BBY.

Section 2 provides a brief review of previous field observations of breaking statistics. Section 3 discusses the present measurements in detail, which describe the experimental site at Lake George, the instrumentation, the data collected, and the methodology used to detect the breakers. Section 4 presents the main results and includes a discussion of the limiting wave height in finite depth water and a comparison with the BBY results for deep water behavior. Section 5 presents our conclusions.

2. Previous Observations

Available field observations of breaking statistics of wind-generated waves are far from comprehensive and are best regarded as fragmentary. Logistical difficulties associated with these observations are increased because the most important situations of extreme seas are usually the least accessible to systematic measurement. Even when reliable wave height data are obtained, the absence of established breaking criteria for such measurements makes it difficult to detect particular breaking events within these data records.

In BBY we provided a detailed review of deep water breaking observations. Previous authors used a variety of field properties, methods, and criteria to detect, trace, and describe breaking properties, probabilities, and statistics. *Wu* [1979] provided a summary of whitecap coverage statistics based on field observations by *Monahan* [1971] and *Toba and Chaen* [1973], who analyzed photographs of the water surface. *Longuet-Higgins and Smith* [1983] detected "jumps" in the rate of change of the elevation signal related to the passage of breaking crests. *Weissman et al.* [1984] analyzed changes of spectral energy in the 18-32 Hz frequency band to detect breaking events. *Ding and Farmer* [1994] used an array of four hydrophones to detect and track breaking waves and thus determine their duration, velocity, and spacing in terms of "active acoustic coverage." In his Loch Ness measurements, *Thorpe* [1992] associated large time derivatives of the signal strength in his sonograph records with the occurrence of breaking wave crests. *Gemmrich and Farmer* [1999] detected breaking waves from a buoy on the basis of air entrainment within breaking waves measured by changes in the electrical conductivity of the water at fixed depths just below the water surface. It is evident that there are empirical thresholds underlying most of these methods and there is no standardization amongst them.

A number of researchers have used visual observa-

tion to monitor breaking events. *Holthuijsen and Herbers* [1986], *Katsaros and Atakturk* [1992], *Stolte* [1992], *Babanin* [1995], and BBY, marked or counted breaking events by visually monitoring wave probes either in situ or by subsequently viewing videotapes made during observational periods. Although subject to human error, this method does not suffer the uncertainties of empirical thresholds and the lack of standardization mentioned above.

Various characteristics and parameters have been used to describe breaking statistics or probabilities. Following BBY, we define the breaking probability b_T for the dominant waves as the mean passage rate past a fixed point of dominant wave breaking events per dominant wave period. This nondimensional quantity is expressed in terms of the main temporal scale of the wave field, making it convenient for comparisons and analysis.

Although fragmentary, deep water observations have provided the basis for a number of analyses of breaking probabilities and a review of progress is given by BBY. A larger volume of literature exists on the subject of depth-limited breaking in the surf zone. Although most of this work relates only to the limiting wave height, some, for example, *Battjes and Janssen* [1978] and *Dally* [1990], also consider energy loss during breaking. To the best of our knowledge, however, analysis of the statistics of breaking events in finite water depth outside the surf zone has not been attempted previously, regardless of the bottom slope. In this case an additional unknown contribution from the bottom interaction adds to the already poorly understood nonlinear dynamics that causes wind-generated waves to break. In this paper we endeavour to accommodate these uncertainties by extending the approach proposed by BBY. We assume that breaking onset in wave groups is driven primarily by nonlinear hydrodynamic processes associated with wave groups, together with additional effects imposed by processes creating shear stresses, by the bottom interaction, and by wind forcing.

Laboratory studies of wave breaking have not been addressed in this brief review because their conformity to field data is questionable. We discuss this further in section 5.

3. Measurements

The finite depth wave-breaking data used in the paper were obtained at our experimental site at Lake George near Canberra in south-eastern Australia (Figure 1) during October-December 1997. A contour map of Lake George, shown in Figure 1, indicates a simple bathymetry, with the bed sloping very gently toward the eastern shore of the lake. Since its bed form is extremely flat, Lake George is an ideal location to study in situ fetch-limited behavior of wind-generated waves in a constant, finite depth environment.

Lake George has been the site of extensive investigations of spectral development of the finite depth waves [*Young and Verhagen*, 1996a, 1996b, *Young et al.*, 1996]. The wave spectrum and meteorological conditions were measured at a series of eight fetch locations ranging from 1.5 to 16 km and a comprehensive data set on fetch-limited wave growth was obtained.

A new experimental site was established recently on Lake George as part of the Office of Naval Research (ONR) Shoaling Surface Waves Project. Since the predominant wind directions at Lake George are westerly and north-westerly, the site was located near the eastern shore as seen in Figure 1. Under typical meteorological conditions the range of values of inverse wave

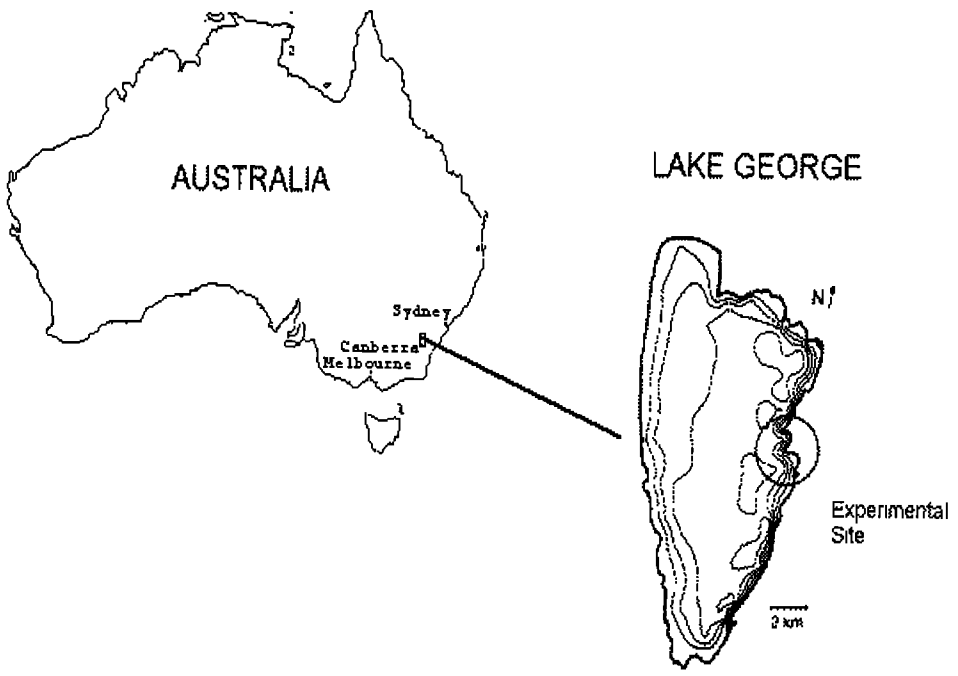

Figure 1. Location of the Lake George site.

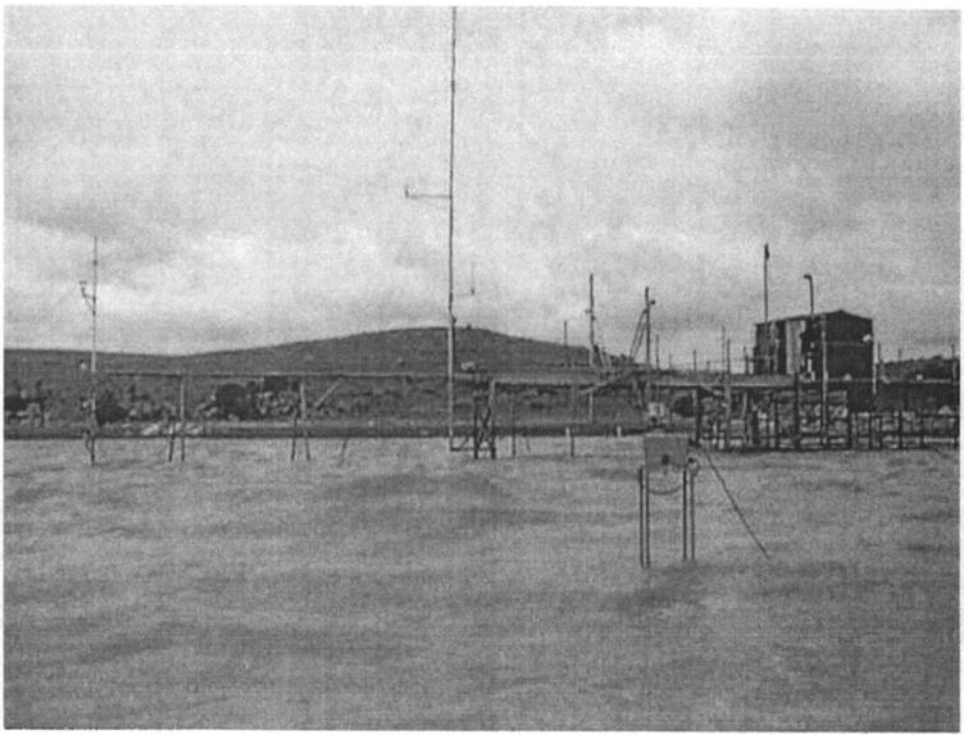

Figure 2. General view of the experimental site at Lake George. The platform and hut containing logging equipment are shown on the right. The measurement bridge extends toward the left.

age U_{10}/c_p and nondimensional depth $k_p h$ expected at the site are $1.0 < U_{10}/c_p < 3.5$ and $0.7 < k_p h < 2.0$, respectively. Here U_{10} is wind speed measured at the standard 10 m height above the water level, c_p and k_p are phase speed and wavenumber corresponding to the spectral peak, and h is the mean water depth. For linear waves these experimental conditions are representative of intermediate depth wind seas.

The experimental site includes an observation platform with a shelter to accommodate equipment and researchers during observational periods (see Figure 2 for a general view). The platform is located 50 m from shore and is accessible via an elevated walkway. The site is equipped with a comprehensive instrumentation system for the study of finite depth wind wave energy sources and sinks. The measurements described in this paper were made from a 10 m long measurement bridge located to the side of the platform (see Figure 2). Approximately halfway along the bridge, the water surface elevation was measured using an array of capacitance gauges. A hydrophone was located directly below the capacitance gauges and sensed the noise generated by individual breaking waves. The water surface around the capacitance gauges and hydrophone was viewed using a video camera. In addition, the records were electronically "marked" by an observer who manually recorded visual occurrences of breaking. All the measurements were synchronized. Using this integrated system, it was possible to interrelate the visual appearance of the water surface in any sequence of individual video frames and the acoustic signature of breaking waves at that time, together with the wave height properties measured by the directional array at the breaking location.

An anemometer mast, accommodating three wind probes at 10 and 5.65 m elevations above the water surface (two cup anemometers and one wind vane), was erected 10 m from the platform beyond the end of measurement bridge to avoid disturbing the air flow. Another anemometer mast, accommodating five wind probes at four heights closer to the surface (four cup anemometers and a wind vane), was set 6 m to the side of the bridge to ensure undisturbed airflow for these lower anemometers.

A total of 26 records of all the measured variables, taken during the measurement period in October- December 1997, were processed, and Table 1 summarizes their parameters. Selection of the records was based only on the requirement of relatively constant wind speed.

The wind speed U_{10} and wind direction were measured very close to 10 m above the water level by the uppermost wind speed and wind direction sensors on the anemometer mast. The wind probes were Aanderaa Instruments wind speed sensor 2740 and wind direction sensor 3590. Slow changes in the water depth in Lake George caused only small variations in the position of the sensors over the surface, and corresponding adjustments in the U_{10} speed were made on the basis of the wind profiles obtained with the anemometer mast.

Table 1. Summary of the Wind-Wave Data

	Run	f_p, Hz	H_s, m	U_{10}, m/s	ϵ	Δ	γ	H_s/h	b_T
1	311501.oc7	0.48	0.21	11.0	0.078	0.509	0.672	0.222	0.016
2	311615.oc7	0.48	0.17	8.5	0.059	0.474	0.517	0.178	0.007
3	311638.oc7	0.49	0.17	9.4	0.062	0.475	0.581	0.183	0.005
4	311757.oc7	0.42	0.35	17.1	0.114	0.496	0.977	0.337	0.375
5	311823.oc7	0.36	0.45	19.8	0.120	0.513	1.035	0.410	0.600
6	311845.oc7	0.33	0.40	15.0	0.096	0.538	0.797	0.372	0.388
7	311908.oc7	0.35	0.37	12.9	0.101	0.500	0.721	0.380	0.279
8	311930.oc7	0.38	0.34	12.8	0.107	0.436	0.723	0.347	0.265
9	311958.oc7	0.39	0.33	11.5	0.100	0.457	0.646	0.324	0.210
10	312021.oc7	0.40	0.39	13.7	0.132	0.397	0.761	0.365	0.303
11	312048.oc7	0.37	0.37	13.1	0.112	0.390	0.718	0.348	0.182
12	312111.oc7	0.40	0.25	9.3	0.074	0.434	0.536	0.290	0.087
13	312207.oc7	0.48	0.20	8.5	0.083	0.399	0.532	0.227	0.047
14	312232.oc7	0.50	0.22	9.0	0.100	0.399	0.568	0.239	0.077
15	312254.oc7	0.49	0.22	9.1	0.092	0.380	0.565	0.240	0.058
16	312316.oc7	0.49	0.21	8.6	0.084	0.384	0.532	0.228	0.086
17	312339.oc7	0.50	0.21	8.6	0.090	0.400	0.541	0.230	0.060
18	010004.no7	0.52	0.22	9.8	0.101	0.396	0.629	0.240	0.113
19	010030.no7	0.48	0.24	10.7	0.106	0.412	0.665	0.266	0.119
20	010055.no7	0.46	0.26	11.8	0.105	0.414	0.723	0.285	0.165
21	010140.no7	0.43	0.28	12.6	0.096	0.461	0.759	0.303	0.157
22	010204.no7	0.40	0.31	13.3	0.105	0.497	0.782	0.332	0.192
23	010226.no7	0.40	0.35	13.9	0.122	0.461	0.810	0.370	0.257
24	010248.no7	0.39	0.35	14.8	0.115	0.479	0.850	0.364	0.271
25	151238.de7	0.48	0.19	11.1	0.067	0.573	0.716	0.227	0.009
26	151301.de7	0.45	0.21	11.8	0.071	0.524	0.737	0.250	0.021

Summary of recorded data. Here, f_p is the spectral peak frequency, H_s is the significant wave height, ϵ is the significant steepness of the spectral peak, Δ is the shear parameter, γ is the non-dimensional peak frequency or the parameter of the inverse wave age, and b_T is the spectral peak breaking probability. The symbols are defined in Section 4.1 below.

Relatively young, strongly forced waves with $U_{10}/c_p = 3.3-6.5$ were observed. Their spectral peak frequencies f_p ranged from 0.33 to 0.50 Hz. The wind speed U_{10} ranged from 8.5 to 19.8 m s^{-1}.

Visual detection of wave breaking occurrence is arguably the most reliable method available since it does not require any additional experimental criteria. At Lake George most wave records were supplemented by videotaped images of the water surface surrounding the wave array. The videotaping allows repeated playback of wave records to establish the breaking statistics by visual means and verification of the results. This visual observation method was used to obtain the breaking statistics in this paper.

As mentioned above, the video records were synchronized with the surface elevation records gathered by the array of wave probes. Both the surface elevation sampling and video framing were performed at 25 Hz so that there was unambiguous correspondence between each wave height reading and a video image. For the video taping a computer-controllable Panasonic model AG-7350 video recorder (VCR) was used whose time code generator facility allowed rapid retrieval of particular segments of the recorded wave series corresponding to visually observed breaking events.

The hydrophone output was recorded on the VCR audio channel. The hydrophone had two signal gains, 20 and 40 dB. Normally, for developed wind waves the 20 dB gain was sufficient to detect breaking waves. During data analysis the acoustic signal was sampled at the 8 KHz rate and digitized. These synchronized time series of the acoustic signal contain potentially valuable additional information about visually observed dominant wave breakers, particularly in relation to breaker strength.

Figure 3 shows a spectrogram of the first minute of record 4 in Table 1. The spectrogram is a time series of consecutive spectral densities computed over 256 readings of the acoustic signal with a 128 point overlap; the segments were windowed with a Hanning window. Values of the spectral density are shown using a logarithmic scale, with darker patches corresponding to higher values (i.e., louder recorded sound levels).

The dark crests across almost the entire 4 KHz frequency span in the spectrogram are associated with acoustic noise from dominant breaking waves. This was confirmed through repeated viewing of the synchronized video records. For example, the first and last breakers (near $t = 1$ s and $t = 55$ s) detected in the spectrogram in Figure 3 are shown in the captured video images seen in Figures 4a and 4b, respectively. It is clear that these are cases when the crest of a breaking wave is passing through the wave array and over the bottom-mounted hydrophone.

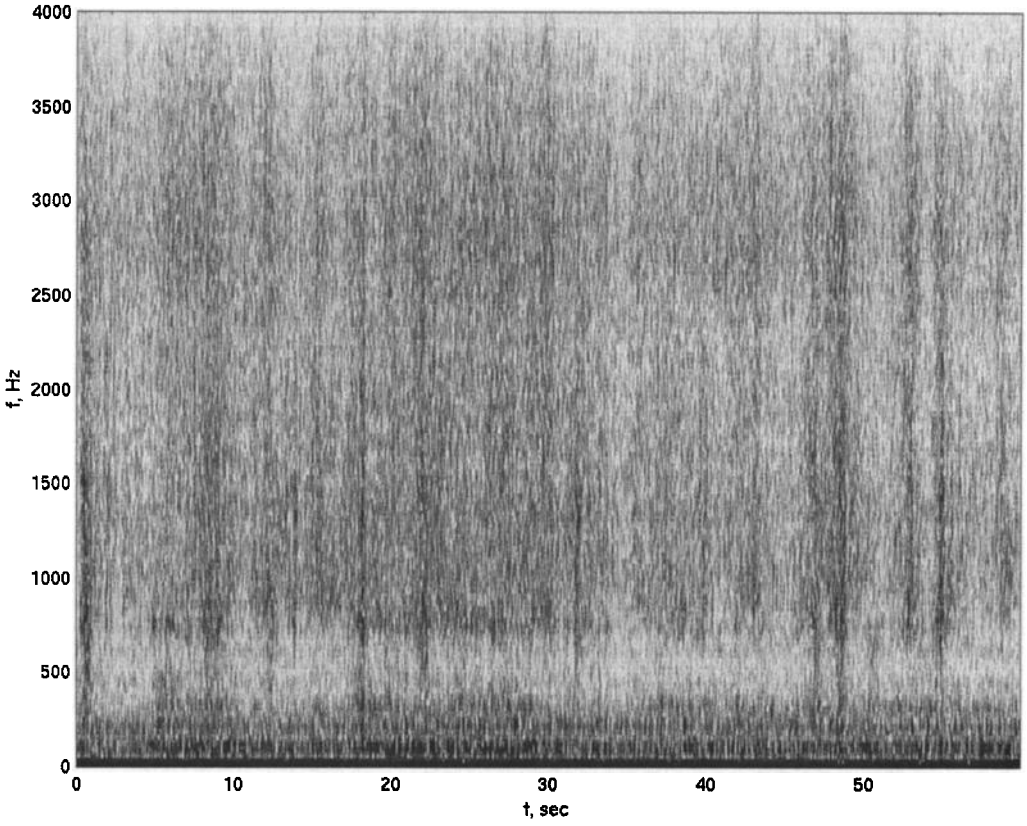

Figure 3. Spectrogram of acoustic noise of the first minute of record 4 (Table 1).

Figures 4c-4f show time series of the digitized acoustic signal near $t = 1$ s and $t = 55$ s. In both Figures 4c and 4d, there are well-defined peaks in the acoustic noise level associated with the breaking events. This is in qualitative agreement with laboratory results, for example, by *Melville et al.* [1992], who concluded that acoustic energy radiated by breaking waves is approximately proportional to the mechanical energy dissipated. In contrast to laboratory breaking waves, different fractions of energy are apparently lost by field breakers, and therefore the breaking noise impact above the background in situ ambient noise is not always evident in field acoustic time series. For instance, the breaking event that occurred at $t = 53$ s of the first minute of record 4 is not well defined in the time series in Figure 4d, although it is seen clearly in the acoustic noise spectrogram in Figure 3.

If the temporal resolution of the acoustic signal is increased, as in Figures 4e and 4f, other features become apparent. For the breaker occurring in the first second (Figure 4e), there is an apparent alteration of the frequency of the sound: the acoustic carrier downshifts in frequency. This is not the case, however, for the breaker at $t = 55$ s (Figure 4f), in spite of the fact that the acoustic signature of this breaker has quite a distinct amplitude enhancement above the ambient noise. Nevertheless, both breakers are clearly seen as breaking crests in the spectrogram in Figure 3.

After we established unambiguously the connection between the spectrogram signatures and the visually observed breakers the acoustic spectrograms were used along with the video records to obtain the breaking statistics for the present paper. Figure 5 shows another example of breaking occurrences during a 1 min segment of record 12 when two isolated breakers occurred within the 1 min record.

Thus the use of spectrograms rather than acoustic intensity time series is the preferred method for detection of dominant breaking events in the wave field. A similar conclusion was reached by *Bass and Hay* [1997], who used spectrograms to detect breakers in the natural surf zone. However, the acoustic time series can provide useful physical insight into the breaking process, i.e., in order to estimate periods of individual breaking waves, the amount of energy lost, etc. [e.g., *Melville et al.*, 1992].

4. Breaking Statistics

As discussed in section 1, additional bottom interaction is imposed on the orbital wave velocities in finite depth environments. This interaction should lead to a modification of the breaking statistics compared to deep water cases for similar circumstances and should result in an increase in the breaking probability.

In the present paper we seek mean breaking occur-

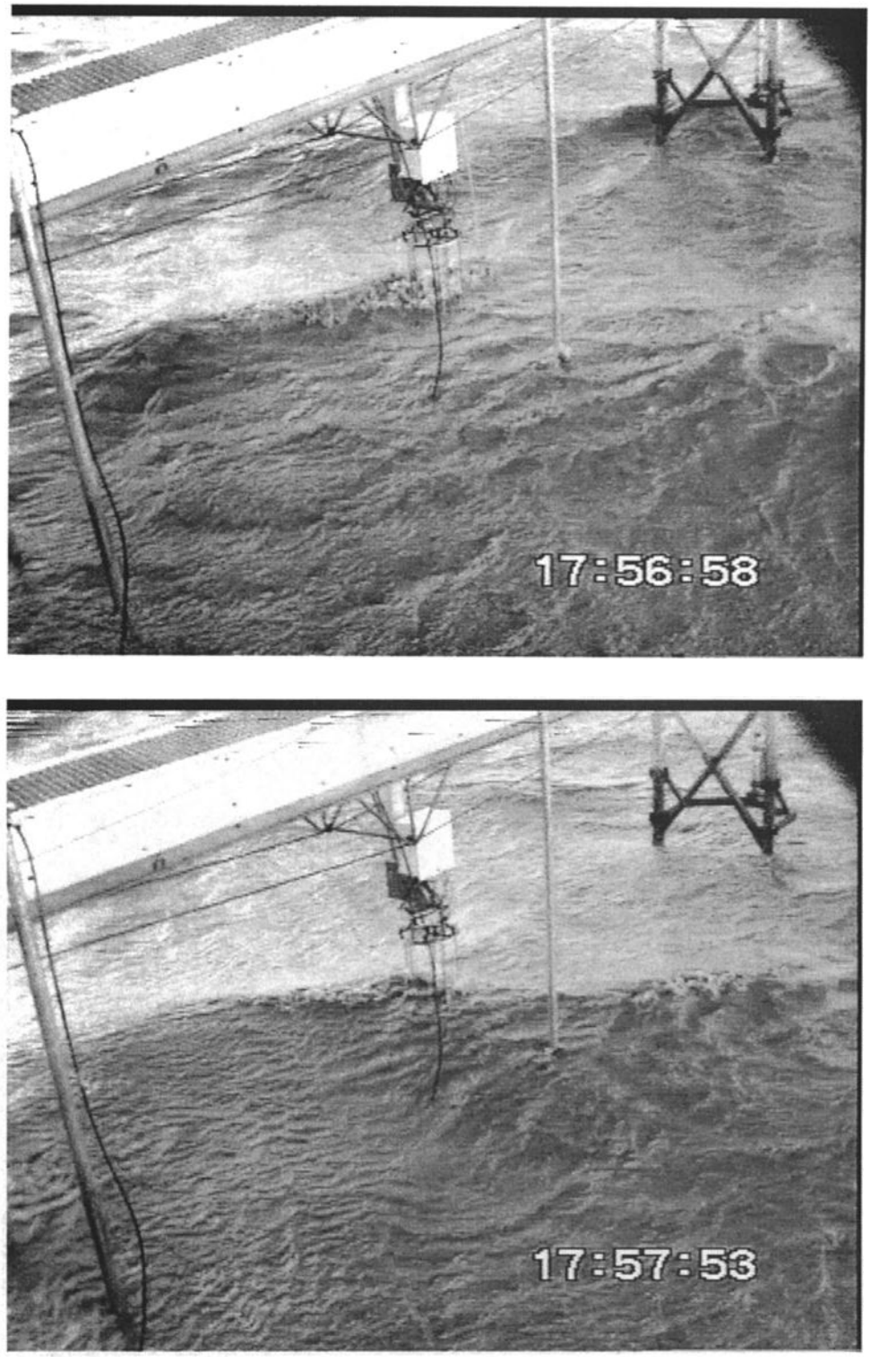

Figure 4. Video images and acoustic signatures of the breakers occured near $t = 1$ s and $t = 55$ s of the first minute of record 4 (Table 1). (a) Video image of the breaker occurring near $t = 1$ s of the record. (b) Video image of the breaker occurring near $t = 55$ s of the record. (c) and (e) Time series of the acoustic noise generated by the Figure 4a breaker . (d) and (f) Time series of the acoustic noise generated by the Figure 4b breaker. The acoustic level scale is arbitrary.

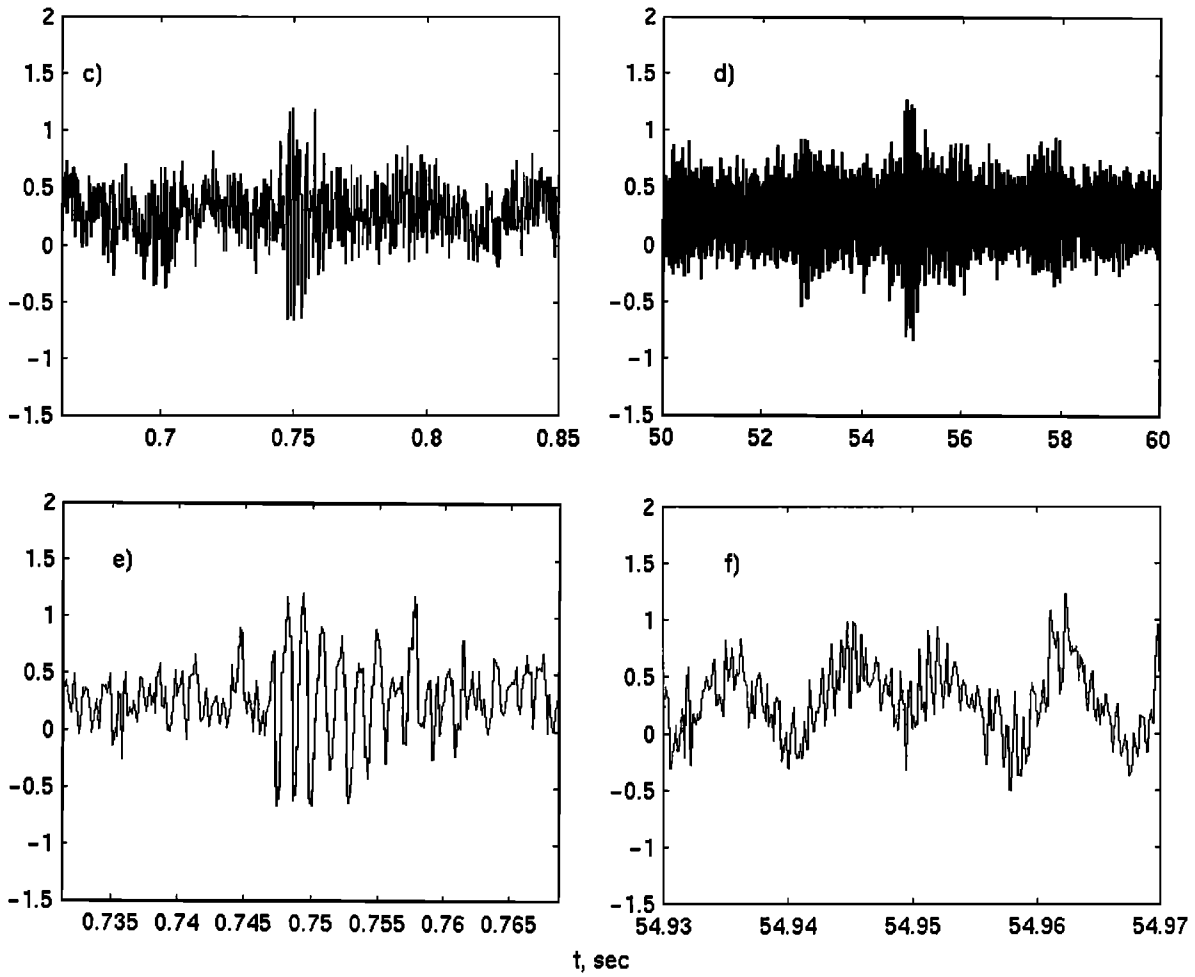

Figure 4. (continued)

rence statistics. However, we shall first discuss the stability of individual high waves in shallow water in order to understand the differences introduced into the breaking process by close proximity of the bottom.

4.1. Height Limits of Individual Waves in Finite Depth Water

Both BBY and the present paper argue that mean wave steepness rather than local steepness or other properties of individual waves determines mean breaking statistics and probability of wave breaking. In this section we discuss how this approach relates to the concept of limiting individual wave height used in the coastal engineering literature.

Nelson [1997] provides an extensive review of limiting wave height data in constant water depth and over mild slopes. He concludes that in water of constant depth, no individual wave can have a H/h ratio exceeding 0.55, but this upper limit may be less. Here H is the height of individual waves. Since the Lake George bottom topography is very flat, according to *Nelson* [1997] we should expect the constant depth limit of $H/h = 0.55$ to apply.

The height of an individual wave is defined as the elevation difference between a wave crest and a wave through. For irregular asymmetric field waves this definition has the uncertainty of whether the height is a zero level up-crossing or a zero level down-crossing wave height. In Figure 6, consecutive wave heights occurring at the wave array during record 5 from Table 1 are shown for both down-crossing (Figure 6a) and up-crossing (Figure 6b) analyses. The $0.55h$ limit is also indicated. This was a case of substantial waves for this site, generated by a 20 m s^{-1} mean wind, with a ratio of the significant wave height H_s to the water depth h of 0.41.

As can be seen in Figure 6, for such an extreme case as record 5 a few waves did exceed the $0.55h$ limit both for the down-crossing and up-crossing heights. In total, 1.4% of the waves were registered as exceeding the $0.55h$ height limit at the measurement site. We investigated these waves in the video records and found that all these waves were breaking while passing through the array. It means that if the evolution of a wave train results in a wave higher than $0.55h$, then that wave will become unstable and break.

As we gradually lowered the wave height threshold level in our analysis, we found that all waves that registered heights of $0.44h$ or greater were breaking. Once

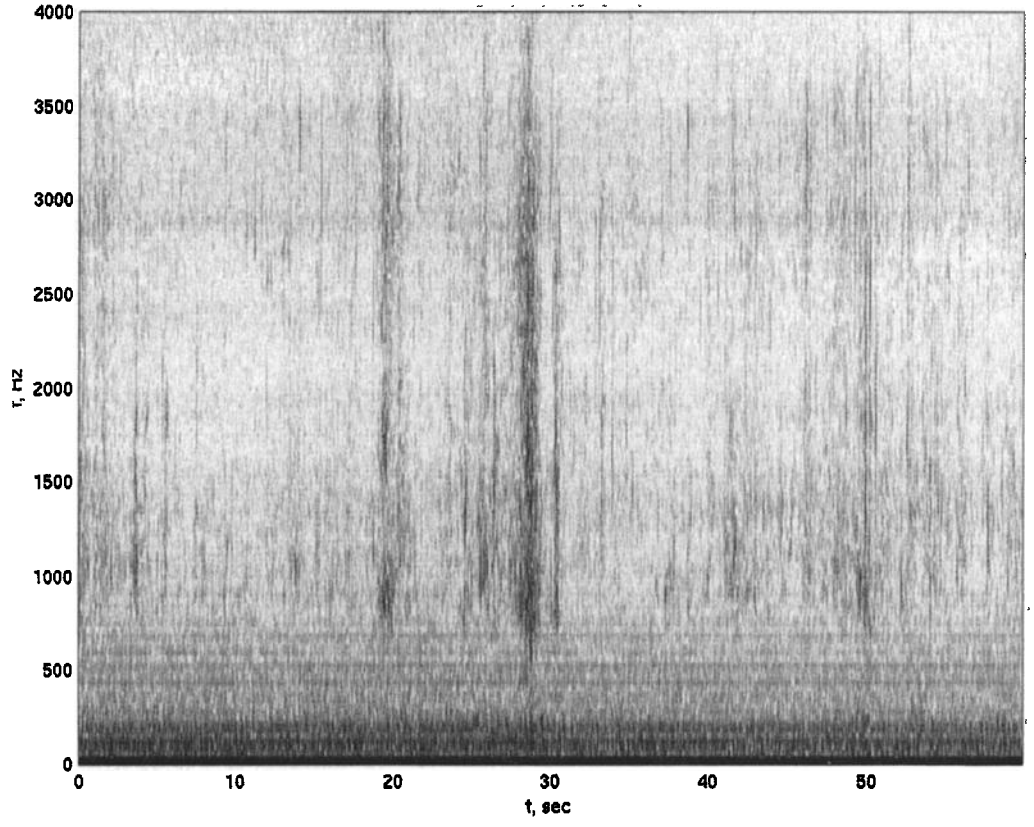

Figure 5. Spectrogram of acoustic noise of the thirty-second minute of record 12 (Table 1).

waves attain this height, they apparently lose their stability because of the bottom interaction. We found, however, that waves lower than $0.44h$ may break or may undergo recurrence. This latter breaking should be controlled by processes similar to those that cause breaking in the deep water, although supplemented by the bottom interaction effects.

In Figure 6 the level of $0.44h$ is shown by the dashed line. A total of 52 waves, or 8.3%, exceeded this level and broke, 18 of which exceeded the limit on both the forward and rear slopes. On many occasions, two consecutive waves exceeded this level and subsequently broke. These waves were associated with the centers of wave groups. However, the 8.3% proportion of breaking waves that can be predicted solely by the ratio of their wave height to the water depth represents only about 14% of the total number of breaking events, even for this extremely wind-forced situation (see Table 1). This means that the majority of breaking events still occurred because of nonlinear hydrodynamical processes in the wave field, similar to those operative for deep water breaking.

Figure 7 shows a consecutive set of wave heights for record 9 of Table 1. Under an 11.5 m s^{-1} wind speed the waves are still quite steep, and 21% of the waves broke. This is a higher proportion than one would expect for a deep water wave field (BBY). However, the ratio of $H_s/h = 0.3$ is small compared to record 5, and only 1.7% of waves exceed the $0.44h$ level. This supports the idea discussed in detail below that although there is a fraction of high waves that lose stability and break because of direct interaction with the finite depth bottom, the majority of breaking events still occur because of nonlinear hydrodynamic forces similar to those operative in deep water.

4.2. Dependence of the Breaking Probability for Finite Depths

As defined by BBY, the breaking probability b_T for the dominant waves is taken as the mean passage rate past a fixed point of dominant wave-breaking events per dominant wave period. The dominant waves are taken within the spectral band of $0.7f_p - 1.3f_p$ (the so-called "spectral peak enhancement region"), which contains the spectral components determining the group structure of the dominant wave field. As it was also noted by BBY, this is a natural choice of bandwidth that allows for wave groups comprising three or more carrier waves.

A strong association of the onset of breaking of dominant waves in deep water with the wave group structure has been documented by a number of authors [see, e.g., *Donelan et al.*, 1972, *Holthuijsen and Herbers*, 1986). In finite water depth this association with wave group structure is also very evident. In Figure 8, four different breaking events relating to various wind-wave circumstances are underlined in our Lake George surface

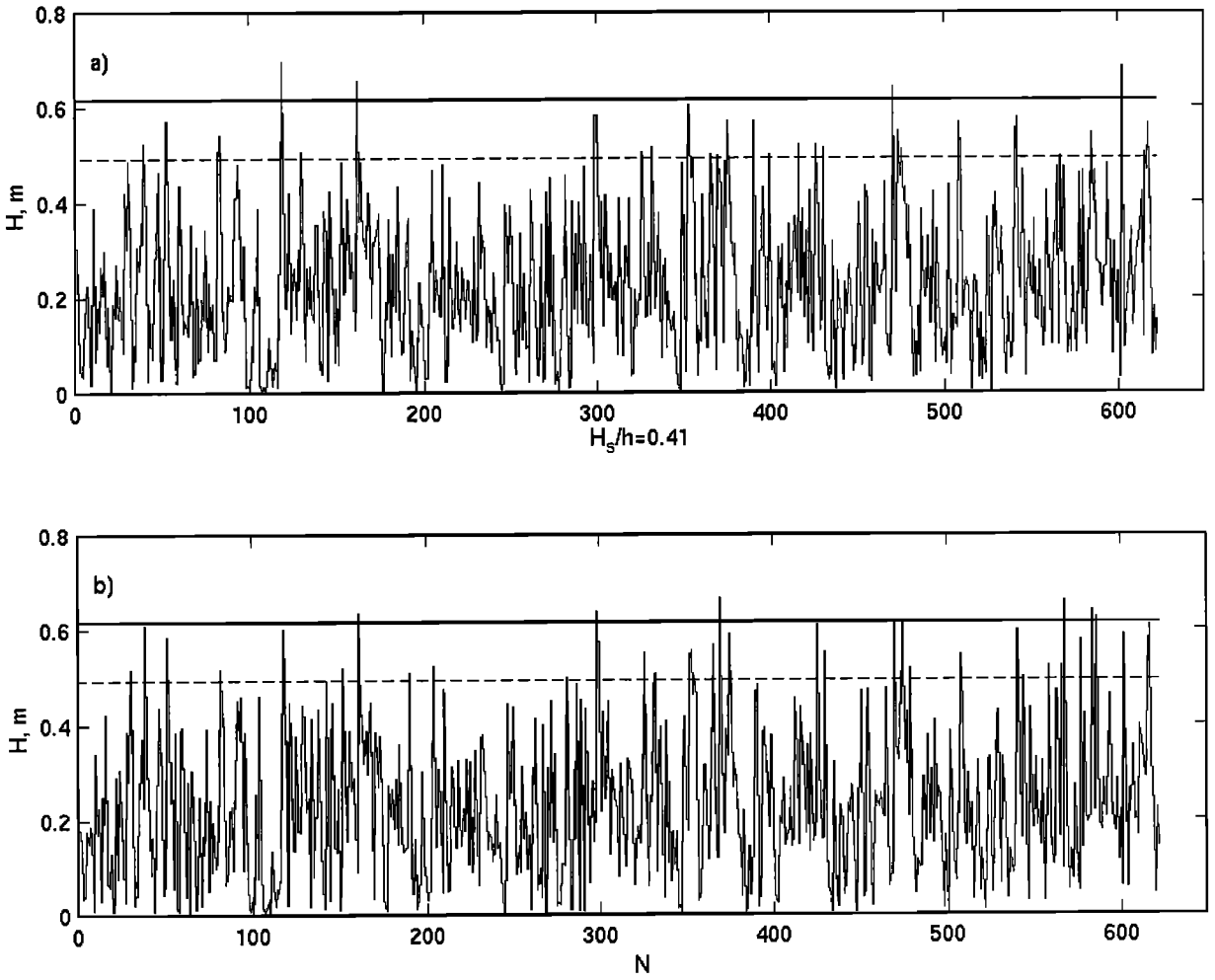

Figure 6. Consecutive (a) down-crossing and (b) up-crossing wave heights of record 5 (Table 1). The horizontal lines indicates the $0.55h$ limit (solid lines) and the $0.44h$ limit (dashed lines). The legend shows the H_s/h ratio.

elevation series. As can be seen, they all occurred close to the maximum of group envelopes.

Following BBY, we have chosen the significant wave steepness of the spectral peak as the key parameter that reflects the fundamental role of wave group dynamics in determining breaking onset. In the present study we focus on the mean breaking statistics, so it is convenient to use parameters relating to average wave field properties, such as wave spectra $F(f)$. The significant mean wave steepness given by $\frac{H_s k_p}{2}$ contains, however, some contribution from the higher-frequency components, so we introduced the significant steepness of the spectral peak

$$\epsilon = \frac{H_p k_p}{2}, \qquad (1)$$

where $H_p = 4[\int_{0.7f_p}^{1.3f_p} F(f)df]^{1/2}$. Intrinsically, ϵ is an appropriate parameter as it provides a direct measure of nonlinearity of the dominant waves. Values of ϵ for the data records of the present paper are given in Table 1.

A wind-driven vertical shear current is usually present in the ocean. *Banner and Tian*'s [1998] calculations indicate that the presence of a superposed linear vertical shear current contributes to breaking onset and marginally reduces the time to breaking. This is also accompanied by a very modest reduction in the local wave slope at breaking. The actual wind-induced surface layer shear is a complex and elusive region for reliable measurements because of the presence of the orbital motions of surface waves as well as the breaking induced current shear [*Terray et al.*, 1999]. For the purpose of the present paper, as by BBY, we seek a surface shear measure that has the correct order of magnitude and is readily estimated from routine measurements. We proceeded from the recent Particle Image Velocimetry (PIV) wind-wave measurements of Peirson and Banner (W.L. Peirson and M.L. Banner, The surface kinematics of micro-scale breaking wind waves, submitted to *Journal of Fluid Mechanics*, 2001), who reported typical values of the surface drift to wind friction velocity $u_s/u_* \sim 0.3$, exclusive of the Stokes drift contribu-

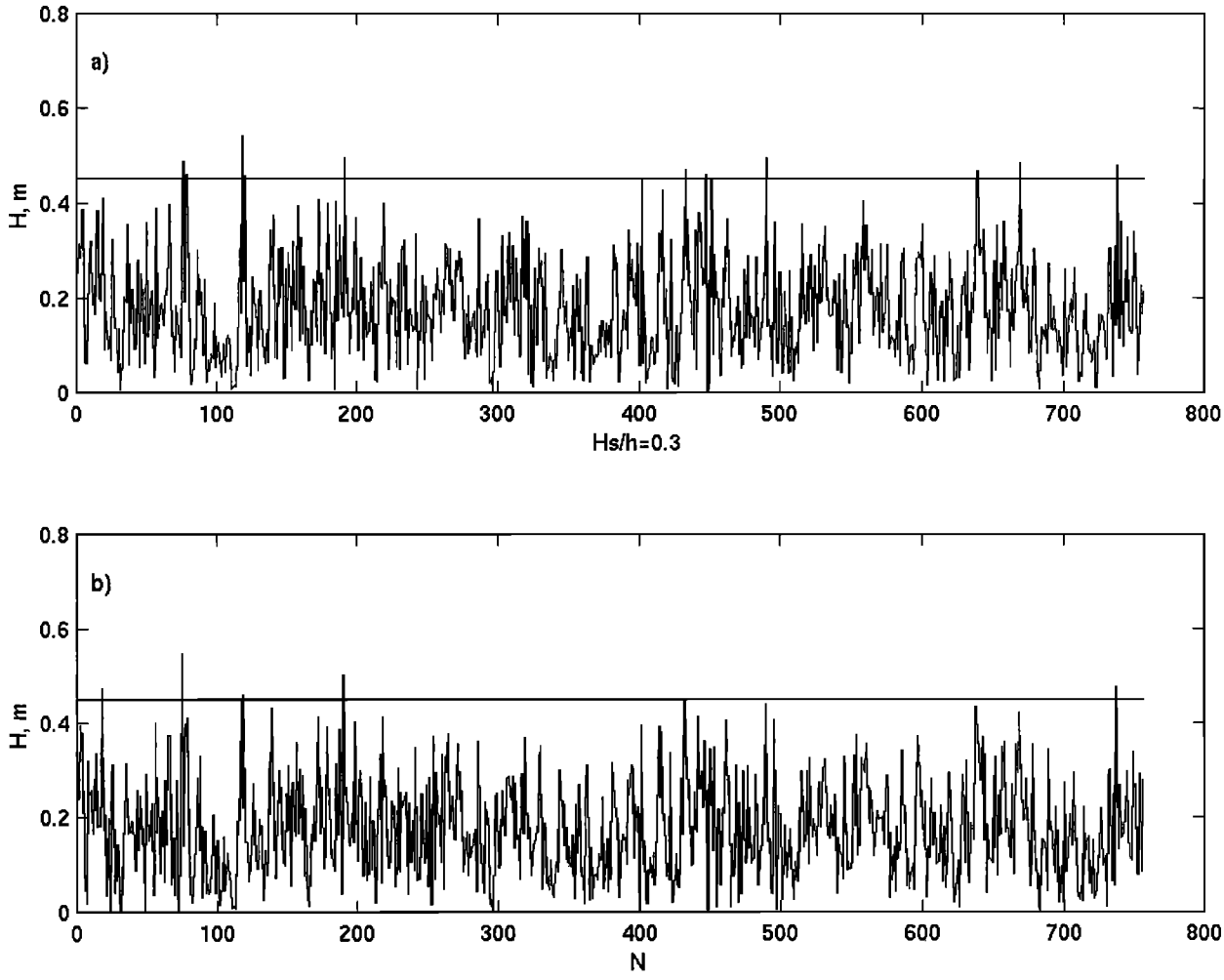

Figure 7. Consecutive (a) down-crossing and (b) up-crossing wave heights of record 9 (Table 1). The horizontal lines indicates the $0.44h$ limit. The legend shows the H_s/h ratio.

tion. On the basis of typical corresponding U_{10} levels we adopted a representative magnitude for the surface layer wind-induced current $u_s \sim 0.01U_{10}$. As an indicative $[O(0.1)]$ parameter to describe the shear current influence on the wave field, we chose Δ, the ratio of the wind-induced surface current u_s to maximum orbital velocity u_0 of a linear surface gravity wave with height equal to the significant wave height:

$$\Delta = \frac{u_s}{u_0} = \frac{0.01U_{10}}{\epsilon c_p}. \quad (2)$$

In regard to the influence of wind forcing our unpublished numerical experiments suggested that it had only a secondary influence on the calculated time to breaking, relative to the unforced case when only nonlinear interactions were operative. As a convenient parameter to quantify the direct influence of the wind forcing in our observations, we used the dimensionless peak frequency

$$\gamma = \frac{U_{10} f_p}{g}, \quad (3)$$

where g is the gravitational constant. Thus γ is an inverse wave age parameter.

To include the influence of the bottom interaction in the independent variable that describes the mean breaking statistics, we chose the ratio H_s/h. This parameter reduces to zero when the water becomes deep or when the waves vanish.

Values of Δ, γ, and H_s/h are also shown in Table 1. In Figure 9 the breaking probabilities b_T are plotted individually against the dominant steepness parameter ϵ and the parameters of the shear current Δ, the wind forcing γ, and the bottom interaction H_s/h. In Figures 9a-9d the breaking probability is seen to be positively correlated with the parameters.

BBY concluded that there is a threshold value of 0.055 for ϵ that determines whether dominant deep water breaking occurs in a wave record. As may be seen in Figure 9a, the data in Table 1 are consistent with this conclusion, and therefore the 0.055 threshold value was adopted for the parameterization in the present paper. To reflect the secondary importance of the shear current and the wind forcing parameters, we incorpo-

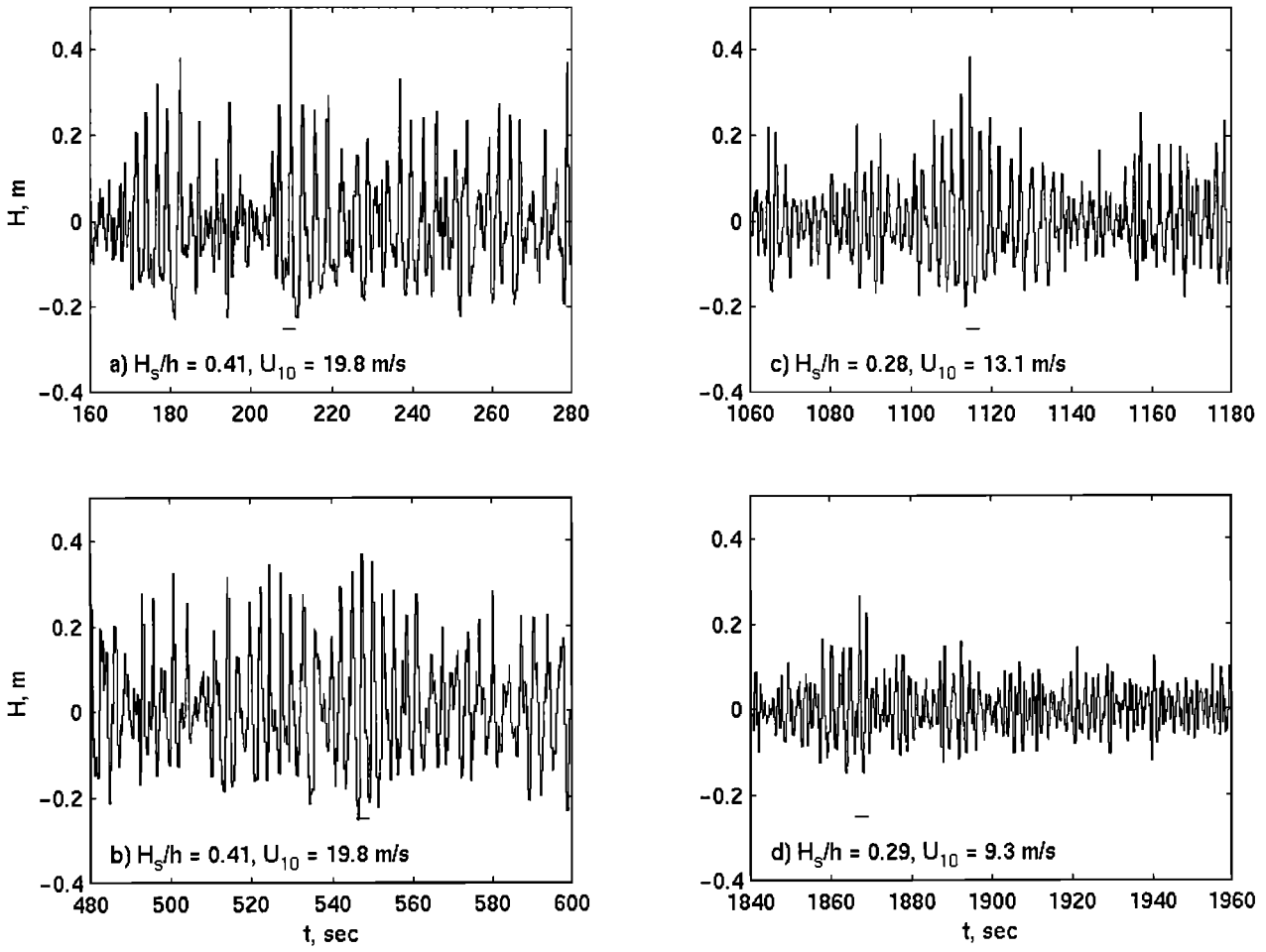

Figure 8. Time series of surface elevations with breaking events underlined. The legend shows the H_s/h ratio and the mean U_{10} wind speed of the records. (a) and (b) Segments of record 5 of Table 1, (c) a record, not documented in Table 1, (d) a segment of record 12 of Table 1.

rated them through assumed linear perturbation terms of the form $(1+\Delta)$ and $(1+\gamma)$, respectively. Accounting for these parameters allows us to improve slightly the resulting correlations and, importantly, to merge the deep water and finite depth dependences. Inclusion of the additional bottom interaction parameter $(1+H_s/h)$ improved the correlation coefficient by about 5% and is also important for merging the deep water and finite depth results. Presumably, this reflects an additional influence of the nonlinearity in the hydrodynamics due to the finite depth, which cannot adequately be expressed through the wave steepness alone. At this point it is not possible to determine the actual mechanism that is operative. One can speculate that it may be the result of different properties of the group structure or changes in the breaking process due to the altered orbital motions in finite depth water. This form, however, allows a simple transition to the deep water case as the water depth becomes large compared to the wave height.

In Figure 10 the dependence of the breaking probability b_T on the dominant wave steepness, adjusted for the finite water depth, is shown plotted on log-log axes. The legend indicates the best fit power law statistics using a standard analysis. The overall power law fit was found to be close to quadratic, with a correlation coefficient of 0.92; 90% confidence intervals are also shown.

The dependence of the spectral peak breaking probability on the composite parameter that includes finite depth, shear current, and wind forcing influence $(\epsilon - 0.55)(1 + H_s/h)(1 + \Delta)(1 + \gamma)$ is shown in Figure 11. Contributions of the latter three terms vanish once the water becomes sufficiently deep and the surface layer shear and the wind input are absent. The correlation coefficient of 0.92 in Figure 11 is the same as in Figure 10. The exponent remains close to quadratic, in agreement with the deep water dependence reported by BBY, and the overall confidence intervals are improved.

4.3. Comparison With Deep Water Data

As was emphasized by BBY and also by this paper, we used physical considerations as the basis for our choice of breaking probability dependences. To validate this approach, the finite depth results of the present paper and the deep water results of BBY should

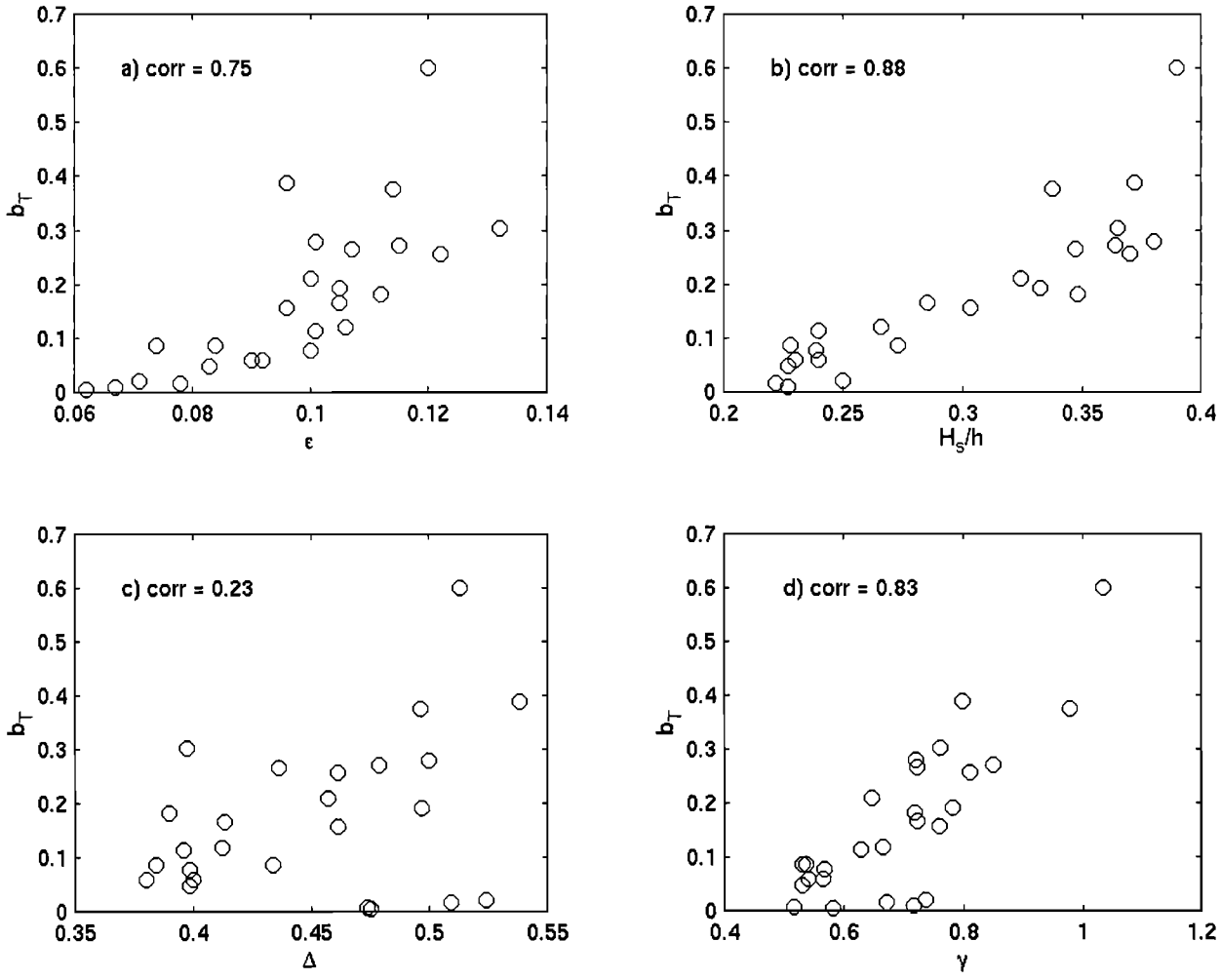

Figure 9. Lake George dominant wave breaking probability b_T versus (a) steepness ϵ (equation (1)), (b) bottom interaction parameter H_s/h, (c) shear stress parameter Δ (equation (2)), and (d) nondimensional peak frequency γ (equation (3)). The legend shows the correlation coefficient based on a linear best fit for each case.

agree closely in spite of the different water depth environments and different scales of waves involved. These factors produce significantly different values of our proposed parameters, and hence this is a stringent requirement. If our choice of parameters was artificial, the overall dependence would be unlikely to fit new data that exceeded the parameter range.

In this case the parameter range of the Lake George data is a significant extension of the deep water data set. While the highest breaking probabilities in deep water were about 10%, this corresponds to nearly the lowest levels in the Lake George set where breaking probabilities reached up to 60%. This comparison of the two data sets provides a stringent test of the conceptual basis underlying our proposed breaking probability dependence.

In Figure 12 the Lake George data are plotted along with the deep water Black Sea, Southern Ocean, and Lake Washington data sets to show the combined data dependence on the dominant wave steepness, adjusted only for finite depth. The finite depth and the deep water data agree quite well, and the overall correlation coefficient of 0.81 is now slightly higher than the 0.78 in Figure 6 of BBY where only deep water data were used.

For the combined depth data sets the dependence of the spectral peak breaking probability b_T on the composite parameter is shown in Figure 13. The data sets agree very well, and the correlation coefficient of 0.89 is very high, particularly if we take into account the diversity of the data used. The exponent is practically quadratic in our final proposed dependence of

$$b_T = 6.63^{+2.05}_{-1.57}[(\epsilon - 0.55)(1 + H_s/h)(1 + \Delta)(1 + \gamma)\}^{1.94^{+0.16}_{-0.12}}, \quad (4)$$

where 90% confidence intervals are shown.

When compared to the proposed dependence in Figure 7 of BBY obtained for deep water data alone, the dependences coincide within the confidence intervals. With the extended data set, the new confidence limits

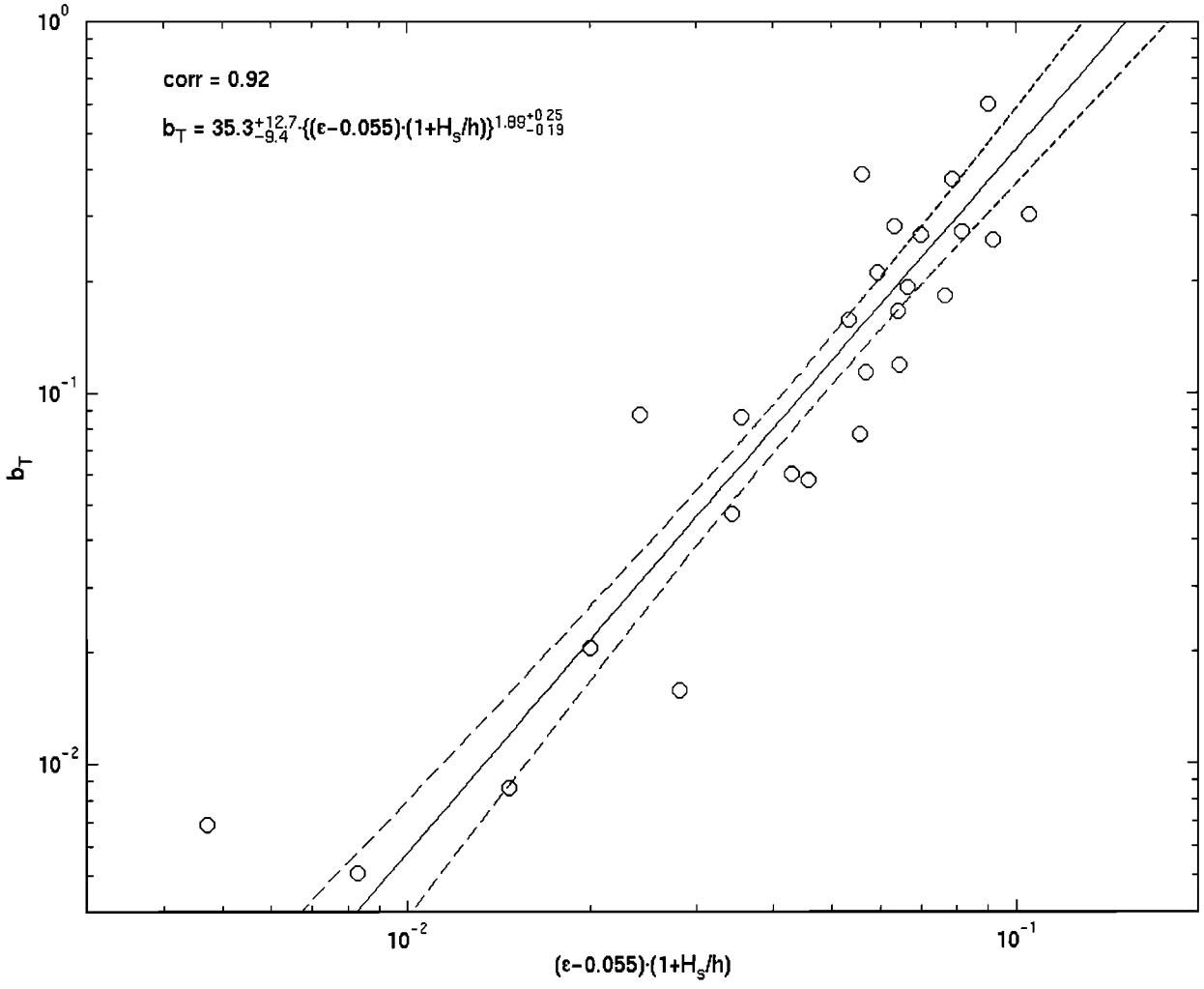

Figure 10. Log-log plot of the observed Lake George dominant wave-breaking probability b_T versus the modified significant wave steepness adjusted for the water depth $(\epsilon - 0.055)(1 + H_s/h)$ (equation (1)). The offset level of 0.055 is the significant peak steepness threshold below which negligible breaking was observed. The legend shows the correlation coefficient based on a linear best fit in the log-log domain together with the coefficients and the ±90% confidence limits.

are narrower. This provides support for the assumptions underlying the choice of parameters for our proposed dependence (4). Equation (4) therefore can be used to predict mean breaking probabilities in the entire parameter range both in deep and finite depth water.

5. Discussion and Conclusions

Our present formulation considers waves traveling over a finite, constant depth layer of fluid. The parameterization would need to be modified to account for sloping bottom topography effects. As our data sets do not include such cases, this extension is left for future studies.

There has been extensive discussion in the literature about the similarity of wind or mechanically forced laboratory waves to waves observed in the field. In regard to the onset of wave breaking it is not clear whether paddle-generated chirped wave groups or waves evolving rapidly at very short fetches under strong wind forcing are undergoing the same dynamical balances as the more slowly evolving wave groups observed in field situations. If these cases are fundamentally different, there may well be significant discrepancies between the breaking probabilities associated with laboratory and field waves.

For example, one of the few available laboratory data sets for intermediate depth breaking, as discussed here, does not appear to be consistent with our field data. Breaking statistics were obtained in the wind-wave tank of the Ocean University of Qingdao, China, by one of the authors (AVB). The water depth in the 1 m wide tank was 0.75 m, and the wind-generated waves were measured at 37.5 m fetch. The breakers were detected at that fetch visually and registered electronically. The relative water depths varied from a quarter to a sixth of

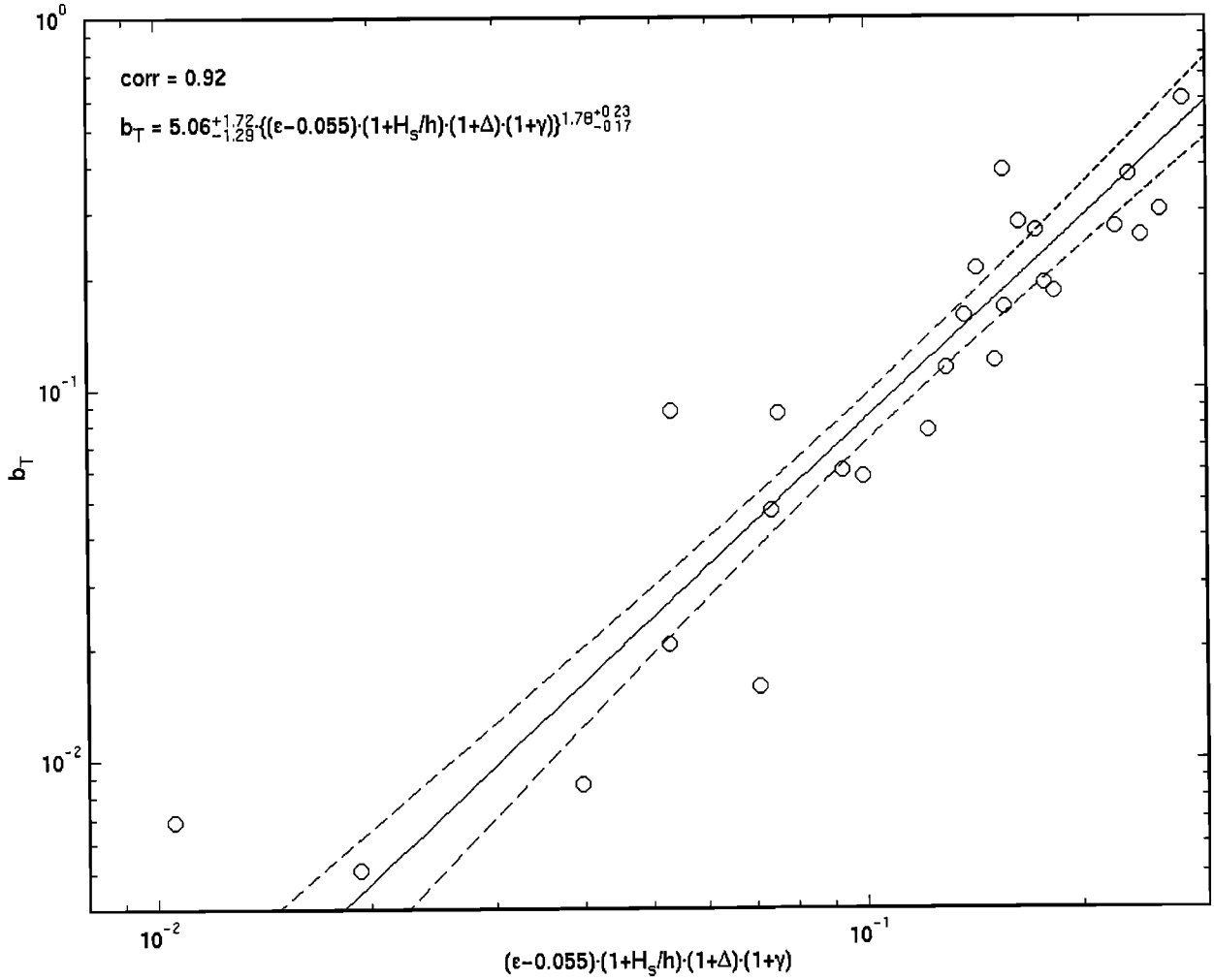

Figure 11. Log-log plot of the observed Lake George dominant wave breaking probability b_T versus the composite parameter adjusted for the water depth $(\epsilon - 0.055)(1 + H_s/h)(1 + \Delta)(1 + \gamma)$ (equations 1, 2, and 3). The legend shows the correlation coefficient based on a linear best fit in the log-log domain together with the coefficients and the ±90% confidence limits.

the wavelength, so that the waves clearly belonged to the intermediate depth class. When plotted together, the Lake George field data and Qingdao (laboratory) observations appear to belong to different populations. We tried other variants of the water depth parameter but could not improve the degree of collapse of these data sets.

Apart from the different dynamical balances of rapidly evolving laboratory wave groups and slowly varying field wave trains and from the possibly differing relative strengths contributed by the wind forcing, laboratory and field waves also have different directional properties. In this respect a recent comparison of two- and three-dimensional wave breaking in the absence of wind forcing was carried out by *Nepf et al.* [1998] in a laboratory experiment. They found that the wave directionality, interpreted as a degree of transverse curvature of wave crests, affects both the onset and severity of breaking events. Although this definition of the directionality is not the same as that in the general field case, one might expect a contribution to the breaking probability due to waves coming from different directions. It is apparent that the directional properties of waves, which may be different in the field and in the laboratory, may alter the process of breaking onset and therefore the statistics of breaking events. Therefore directionality may also need to be included explicitly in the breaking probability dependence. This aspect, however, is also left to future studies.

Finally, we summarize our main findings and conclusions of the present paper.

1. Spectrograms of acoustic noise, recorded with a hydrophone and associated with the waves, can be used to detect wave-breaking events as reliably as visual observation. The acoustic signatures of breaking dominant waves span the frequency band from 500 Hz up

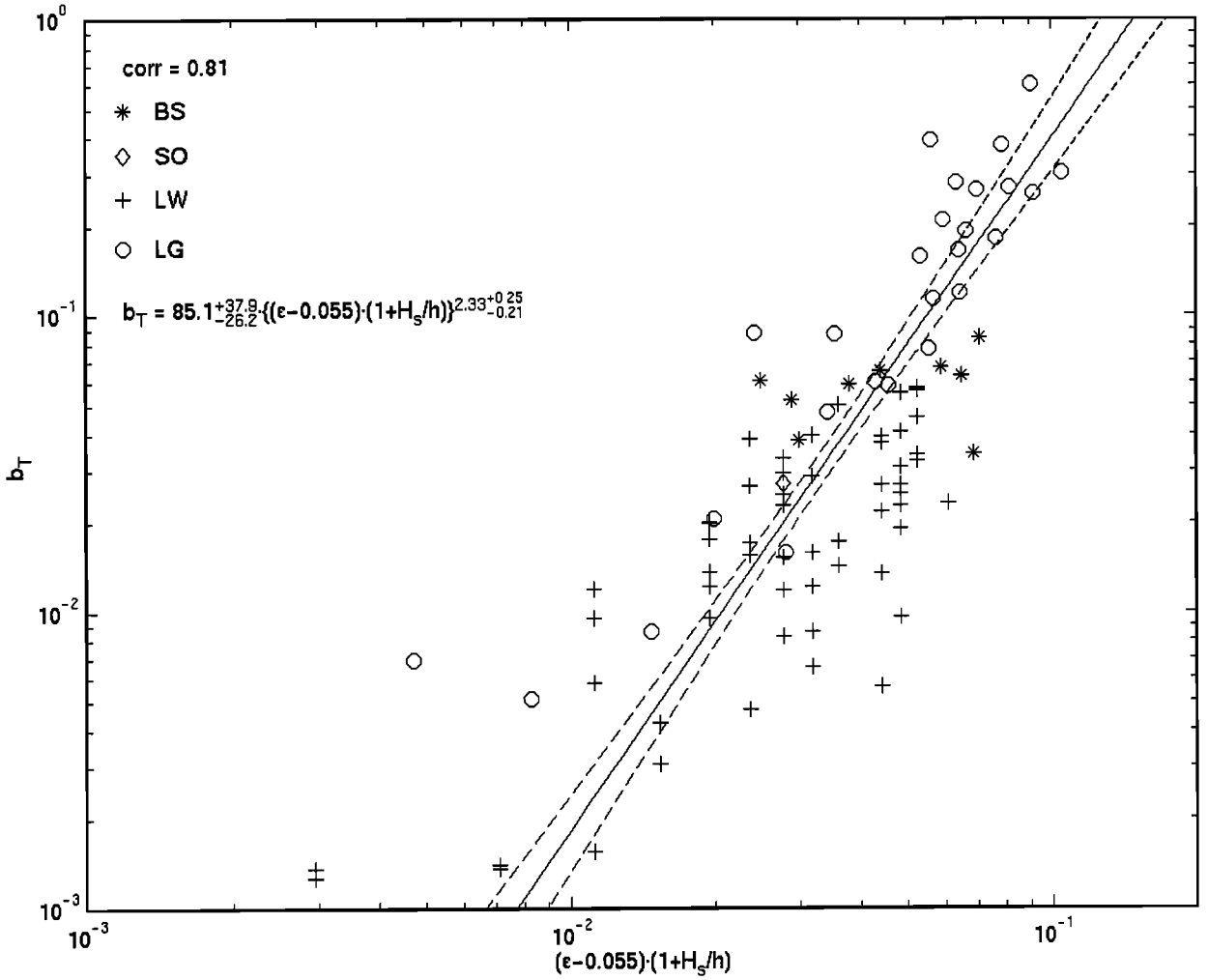

Figure 12. Combined log-log plot of the observed dominant wave breaking probability b_T versus the modified significant peak steepness adjusted for the water depth $(\epsilon - 0.055)(1 + H_s/h)$ (equation 1). Four diverse field sites are shown: Black Sea (BS), Southern Ocean (SO), Lake Washington (LW) (all deep water), and Lake George (LG) (finite depth). The legend shows the correlation coefficient based on a linear best fit in the log-log domain together with the coefficients and the ±90% confidence limits.

to 4 KHz and are seen clearly in the time series of the concomitant spectral densities of the underwater sound.

2. Over a flat bottom the bottom interaction causes waves of height $0.44h$ and higher to break, whereas waves less than $0.44h$ in height undergo random breaking and may either break or not. The number of waves exceeding the $0.44h$ limit depends on the global wave steepness of the wave field, but even in extremely steep cases, the majority of breaking appears to be associated with nonlinear wave group hydrodynamics.

3. The results of BBY provided significant support for their proposition that dominant wave breaking in deep water is driven primarily by nonlinear hydrodynamical processes associated with wave groups, with secondary influences due to the wind drift layer shear current and wind forcing. In the present paper this hypothesis was applied to the dominant waves in a finite depth environment. The parameter $(1 + (H_s/h))$ was used to extend the dependences proposed by BBY to include additional nonlinearity effects due to finite water depth and to allow the merging of deep water and shallow water cases. The quadratic dependence (4) reported in the present paper provides a means to predict the mean probability of dominant breakers for both deep water and finite depth environments.

4. This approach allowed us to combine data from diverse natural bodies of water and from different environments with a correlation coefficient reaching close to 90%. It is, however, noted that the residual scatter may not be statistical variability alone but may have physical origins. In Figure 8 of BBY, it was noted that the record lengths required to describe properly mean breaking statistics need to be considerably longer than those usually adopted in recording wave spectra, as the

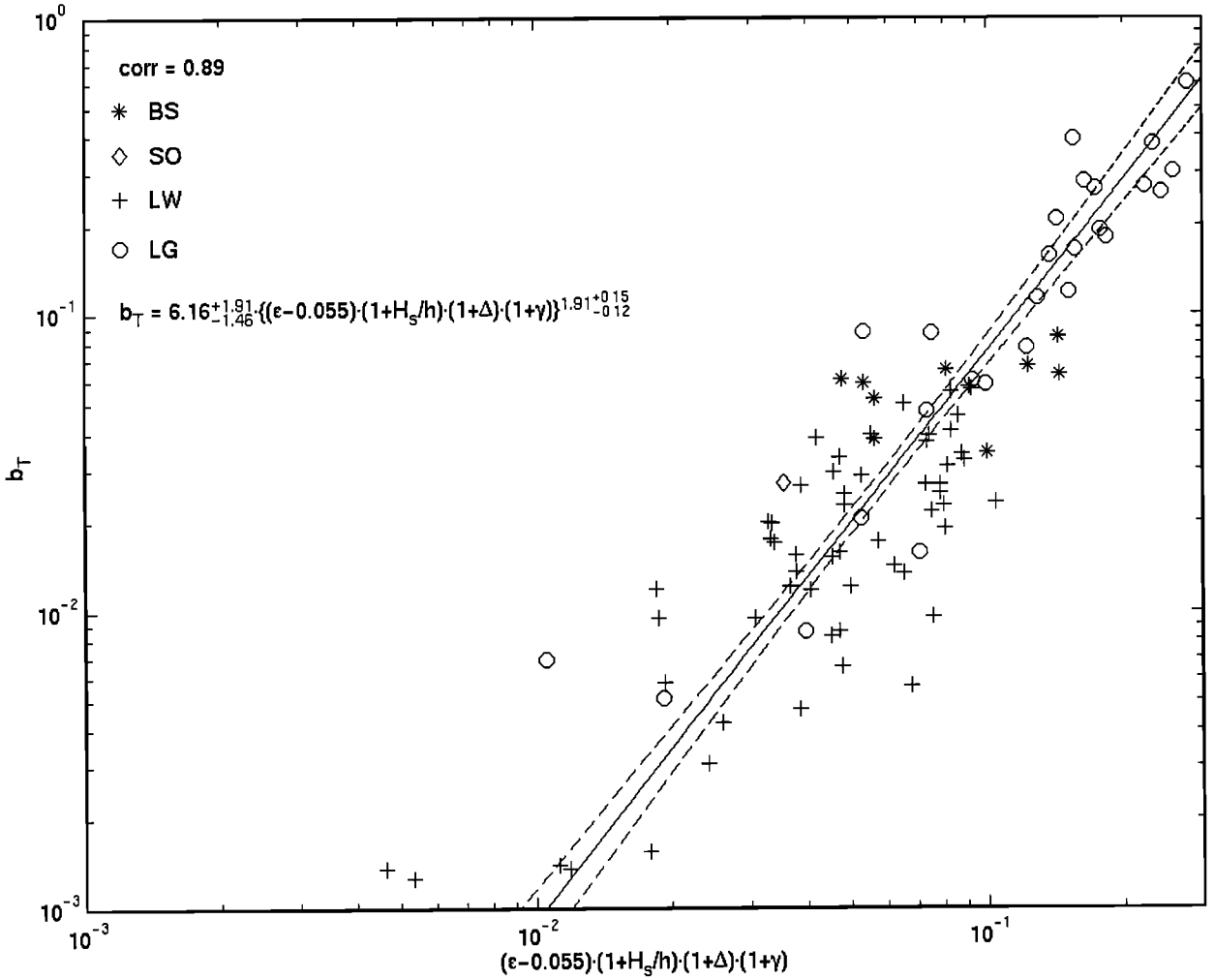

Figure 13. Combined log-log plot of the observed dominant wave breaking probability b_T versus the composite parameter adjusted for the water depth $(\epsilon - 0.055)(1 + H_s/h)(1 + \Delta)(1 + \gamma)$ (equations 1, 2, and 3). Four diverse field sites are shown: Black Sea (BS), Southern Ocean (SO), Lake Washington (LW) (all deep water) and Lake George (LG) (finite depth). The legend shows the correlation coefficient based on a linear best fit in the log-log domain, together with the coefficients and the ±90% confidence limits.

longer timescale associated with unsteady wave groups is involved. In addition, we may need to include a parameter for the wave directionality to reduce the scatter of the breaking data. Verification and quantification of these aspects will require further observational effort, both field and laboratory, and is left to future studies.

Acknowledgments. The authors gratefully acknowledge the financial support of the Australian Research Council and the U.S. Office of Naval Research. The authors also express their appreciation to members of technical staff of the School of Civil Engineering, Australian Defence Force Academy: Jim Baxter, Mary Dalton, Michael Lanza, John MacLeod, Peter McMahon, Bernard Miller, Karl Shaw, Ian Shepherd, and Michael Wilson, who assisted with the experiment at Lake George. We are also very grateful to Prof Wen Sheng Chang and his research group at the Ocean University of Qingdao for their assistance with the laboratory experiment on the breaking statistics of shallow water waves.

References

Babanin, A.V., Field and laboratory observations of wind wave breaking, in *Second International Conference on the Mediterranean Coastal Environment*, vol.3, edited by E. Ozhan, pp. 1919-1928, Autoritat Potuaria de Tarragona, Spain, 1995.

Banner, M.L., and X. Tian, On the determination of the onset of wave breaking for modulating surface gravity water waves, *J. Fluid Mech., 367*, 107-137, 1998.

Banner, M.L., A.V. Babanin, and I.R. Young, Breaking probability for dominant waves on the sea surface, *J. Phys. Oceanogr., 30*, 3145-3160, 2000.

Bass, S.J., and A.E. Hay, Ambient noise in the natural surf zone: wave-breaking frequencies, *IEEE. Oceanic Eng., 22*, 411-424, 1997.

Battjes, J.A., and J.P.F.M. Janssen, Energy loss and set-up due to breaking of random waves, paper presented at 16th Coastal Engineering Conference, Am. Soc. of Civ. Eng., Hamburg, Germany, 1978.

Dally, W.R., Random breaking waves: A closed-form solution for planar beaches, *Coastal Eng., 14*, 233-263, 1990.

Ding, L., and D.M. Farmer, Observations of breaking surface wave statistics, *J. Phys. Oceanogr., 24*, 1368-1387, 1994.

Dold, J.W., and D.H. Peregrine, Water-wave modulations, paper presented at 20th International Conference on Coastal Engineering, Am. Soc. of Civ. Eng., Taipei, China, 1986.

Donelan, M.A., M.S. Longuet-Higgins, and J.S. Turner, Whitecaps, *Nature, 239*, 449-451, 1972.

Gemmrich, J.R., and D.M. Farmer, Observations of the scale and occurrence of breaking surface waves, *J. Phys. Oceanogr., 29*, 2595-2606, 1999.

Holthuijsen, L.H., and T.H.C. Herbers, Statistics of breaking waves observed as whitecaps in the open sea, *J. Phys. Oceanogr., 16*, 290-297, 1986.

Katsaros, K.B., and S.S. Atakturk, Dependence of wave-breaking statistics on wind stress and wave development, in *Breaking Waves*, edited by M.L. Banner and R.H.J. Grimshaw, pp. 119-132, Springer-Verlag, New York, 1992.

Longuet-Higgins, M.S., and N.D. Smith, Measurement of breaking waves by a surface jump meter, *J. Geophys. Res., 88*, 9823-9831, 1983.

Melville, W.K., M.R. Loewen, and E. Lamare, Sound production and air entrainment by breaking waves: A review of recent laboratory experiments, in *Breaking Waves*, edited by M.L. Banner and R.H.J. Grimshaw, pp. 139-146, Springer-Verlag, New York, 1992.

Monahan, E.C., Oceanic whitecaps, *J. Phys. Oceanogr., 1*, 139-144, 1971.

Nelson, R., Height limits in top down and bottom up wave environments, *Coastal Eng, 32*, 247-254, 1997.

Nepf, H.M., C.H. Wu, and E.S. Chan, A comparison of two- and three-dimensional wave breaking, *J. Phys. Oceanogr., 28*, 1496-1510, 1998.

Stolte, S., Wave breaking characteristics deduced from wave staff measurements, *Forschungsanstalt der Bundeswehr fur Wasserschall- und Geophys. Rep. FB 1992-4*, 21 pp., Kiel, 1992.

Terray, E.A., W.M. Drennan, and M.A. Donelan, The vertical structure of shear and dissipation in the ocean surface layer, in *The Wind-Drwen Air-Sea Interface*, edited by M.L. Banner, pp. 239-245, Univ. of New South Wales, Sydney, 1999.

Thorpe, S.A., Bubble clouds and the dynamics of the upper ocean, *Q. J. R. Meteorol. Soc., 118*, 1-22, 1992.

Thorpe, S.A., and P.N. Humphries, Bubbles and breaking waves, *Nature, 283*, 463-465, 1980.

Toba, Y., and M. Chaen, Quantitative expression of the breaking of wind waves on the sea surface, *Rec. Oceanogr. Works Jpn., 12*, 1-11, 1973.

Weissman, M.A., S.S. Atakturk, and K.B. Katsaros, Detection of breaking events in a wind-generated wave field, *J. Phys. Oceanogr.*, 14, 1608-1619, 1984.

Wu, J., Oceanic whitecaps and sea state, *J. Phys. Oceanogr., 9*, 1064-1068, 1979.

Xu, D., P.A. Hwang, and J. Wu, Breaking of wind-generated waves, *J. Phys. Oceanogr., 16*, 2172-2178, 1986.

Young, I.R., and L.A.Verhagen, The growth of fetch limited waves in water of finite depth, part I, Total energy and peak frequency, *Coastal Eng., 29*, 47-78, 1996a.

Young, I.R., and L.A.Verhagen, The growth of fetch limited waves in water of finite depth, part II, Spectral evolution, *Coastal Eng., 29*, 79-100, 1996b.

Young, I.R., L.A.Verhagen, and S.K.Khatri, The growth of fetch limited waves in water of finite depth, part III, Directional spectra, *Coastal Eng., 29*, 101-122, 1996.

A. V. Babanin, Department of Civil and Environmental Engineering, Adelaide University, Adelaide 5005, Australia. (e-mail: alex.babanin@adelaide.edu.au)

M. L. Banner, School of Mathematics, The Univesity of New South Wales, Sydney 2052, Australia. (e-mail: m.banner@unsw.edu.au)

I. R. Young, Faculty of Engineering, Computer and Mathematical Sciences, Adelaide University, Adelaide 5005, Australia. (e-mail: ian.young@adelaide.edu.au)

(Received January 11, 2000; revised August 22, 2000; accepted September 27, 2000.)